

Fouling mechanisms during protein microfiltration: The effects of protein structure and filtration pressure on polypropylene microporous membrane performance

Mina Ahsani^{1,2}, Meisam Dabiri Havigh^{1,2}, Reza Yegani^{*1,2}

¹Faculty of Chemical Engineering, Sahand University of Technology, Tabriz, Iran

²Membrane Technology Research Center, Sahand University of Technology, Tabriz, Iran

Received: 27 June 2016, Accepted: 16 October 2016

ABSTRACT

A polypropylene microporous membrane (PPMM) was fabricated by thermally induced phase separation (TIPS) method. The effects of protein size and structure as well as filtration pressure on the membrane performance and fouling mechanisms were investigated using two different proteins, bovine serum albumin (BSA) and collagen, in dead-end filtration setup. Obtained results showed that, for each protein filtration, increasing the operational pressure led to higher irreversible fouling ratio (IFR) and consequently lower flux recovery (FR). Moreover, in collagen filtration, the higher portion of the total fouling ratio (TFR) belonged to reversible fouling ratio (RFR) and the FR of membrane in collagen solution filtration was higher than that in BSA solution filtration at the same operational pressure. The FR values were about 42.48 and 56.32% at 2 bar, 52.28 and 64.53% at 1.5 bar and 65.97 and 75.83% at 0.75 bar for BSA and collagen solutions filtrations, respectively. Investigation of the fouling mechanisms using Hermia's models showed that the cake filtration mechanism of fouling turned to pore blocking mechanism in both proteins filtrations by increasing the operational pressure. Obtained results using combined fouling models for all filtration processes confirmed that the cake filtration-standard blocking model (CFSBM) was the prevailing mechanism, whilst the contribution of standard blockage increased by increasing the operational pressure. **Polyolefins J (2017) 4: 175-189**

Keywords: Polypropylene membrane; bovine serum albumin (BSA); collagen protein; Hermia's fouling models; combined fouling models.

INTRODUCTION

Membrane is at the heart of every membrane process and can be considered as a permselective barrier or interphase between two phases. Separation is achieved because the membrane has the ability to transport one component from the feed mixture more readily than any other components [1]. Even though ceramic, metal and liquid membranes are gaining more importance,

the majority of membranes are and will be made from solid polymers. In general, this is due to the wide variety of barrier structures and properties, which can be designed by polymer materials [2]. Most commercial membranes are made from polysulfone (PSf), polyethersulfone (PES), polypropylene (PP), polyethylene (PE), and polyvinylidenefluoride (PVDF) due to their excellent chemical resistance, thermal as well as mechanical properties [3]. PP is superior compared to

* Corresponding Author - E-mail: ryegani@sut.ac.ir

many other polymers in mechanical strength, chemical stability, thermal and chemical resistance, and low cost. Therefore, PP is a very promising material for using in separating membranes [4-6]. There are several ways to prepare porous polymeric films, such as sintering, stretching and track etching. Most techniques used for preparation of membranes, however, are carried out by controlled phase separation [7]. Phase separation of polymer solutions can be induced by several ways such as thermally induced phase separation (TIPS), non-solvent induced phase separation (NIPS), evaporation induced phase separation (EIPS), and vapor induced phase separation (VIPS) [2, 8]. Membrane separation processes are currently applied in various fields such as water and wastewater treatment, medicine, pharmacy, and food and beverage industries [9-14]. Recently, membrane-based processes such as microfiltration (MF), ultrafiltration (UF), nanofiltration (NF), membrane chromatography, and membrane contactors have gained importance in biotechnology due to their ability for protein separation and purification [15-21].

They are very well suited to the processing of biological molecules since they operate at relatively low temperatures and pressures and require no phase changes or chemical additives, thereby minimize the extent of denaturation, deactivation, and/or degradation of biological products [22]. Although all membrane processes are essentially used for protein separation/purification, the greatest interest has been directed toward the application of pressure-driven processes using MF, UF and NF systems [23]. MF is widely used for the separation and purification of protein-containing solutions, e.g. for the recovery of extracellular proteins produced via fermentation and for the removal of bacteria and/or viruses in the final formulation of therapeutic proteins [15]. Membrane fouling, however, is one of the major limitations to practical application of membrane processes. Membrane fouling is usually defined as a process in which solutes or suspended particles are deposited on a membrane surface or into the membrane pores during membrane filtration or operation of membrane bioreactors, which results in degradation of the membrane performance. In other words, fouling is a major obstacle against the widespread use of membrane technology. It also causes severe flux decline

and deterioration of membrane performance, which affect the quality of the produced/recycled water. The IUPAC working party on membrane nomenclatures has defined "fouling" as "the process resulting in loss of performance of a membrane due to deposition of suspended or dissolved substances on its external surfaces, at its pore openings, or within the pores" [24]. Fouling is a complicated phenomenon which is seriously affected by such operating conditions as transmembrane pressure, cross-flow velocity and temperature, feed characteristics such as foulant type and size, foulant concentration and feed pH and finally membrane properties such as hydrophilicity/hydrophobicity, roughness, pore size and pore type [18, 25].

Generally, four mechanisms are introduced for membrane fouling during membrane filtration, consisting of cake filtration, complete blocking, intermediate blocking and standard blocking [26]. In the case of cake filtration mechanism, foulants form a layer on the membrane surface. This layer grows with time and causes further flux decline [12]. For complete blocking mechanism, it is assumed that particles seal off pore entrances and prevent flow. Intermediate blocking is similar to complete blocking but it is assumed that a portion of the particles seal off pores and the rest accumulates on the top of other deposited particles [27]. Standard blocking, which also called internal pore blocking, occurs when small size solutes deposit or adsorb onto the pore walls in the membrane [28]. It takes place when the sizes of solutes are less than the size of the pore entrance [29]. These mechanisms may occur individually or in combinations of two or more mechanisms.

Several mathematical models have been derived and introduced by researchers to determine the fouling mechanisms during membrane filtration processes. Hermia's models [30] are the most well-known models which have been used over the years to investigate the fouling mechanisms during constant pressure dead-end filtration processes [29, 31, 32]. In Hermia's models, it is assumed that single fouling mechanism prevails throughout the filtration. However, different studies have reported a transition in fouling mechanism during the course of filtration. For this reason, some combined models have been recently derived and introduced. Bolton et al. [27] derived fouling

models from Darcy's law that accounted the combined effects of the different individual fouling mechanisms. These fouling models are relatively new but have already attracted much attention of several researchers due to their simple application and well agreement with experimental flux decline data [33-35].

In this study, polypropylene microporous membrane is fabricated via TIPS method. The BSA and collagen proteins solutions were filtered using fabricated membrane at different operational pressure and the effects of the foulant type and structure as well as filtration pressure on the membrane performance and fouling mechanisms were investigated. Hermia's and newly presented combined fouling models were used to investigate and analyze the fouling mechanism during each filtration process.

It should be noted that, most fouling studies have been conducted by applying UF membranes [16, 36, 37] and only a few studies have been devoted to protein interaction with MF membranes [23]. Therefore in this work, valuable information has been reported to indicate the protein type and operation pressure effects on the polypropylene microporous membrane fouling and performance during microfiltration process of proteins.

Theory

Hermia's models

The mode of permeate flux decline during filtration process can be identified by the following equation [30]:

$$\frac{d^2t}{dV^2} = \beta \left(\frac{dt}{dV} \right)^n \quad (1)$$

where V is the cumulative volume of filtrate, t is the time of operation and β is a constant. The permeate flux is presented as [32]:

$$J = \frac{1}{A} \frac{dV}{dt} \quad (2)$$

which can be written as:

$$\frac{dt}{dV} = \frac{1}{AJ} \quad (3)$$

Taking derivative of Eq 3 with respect to t and substituting in Eq. 1, we obtain the governing equation of flux decline with time as follow [32]:

$$\frac{dJ}{dt} = -\alpha J^{3-n} \quad (4)$$

where α is a constant and n is a general index which depends on fouling mechanism. The values of n are 2, 1.5, 1 and 0 for complete pore blocking, standard pore blocking, intermediate pore blocking, and cake filtration, respectively. The analytical solutions of Eq. 4 for each n value as well as the linear forms of flux expressions are listed in Table 1 [38].

Combined models

Ho and Zydney [39] developed the first combined model that described the membrane fouling transition by using a single mathematical expression. The model has three fitted parameters and the flux decline, as a function of time, is obtained by approximate solution without integrating. Bolton et al. [27] expanded Ho and Zydney's modeling work by using a new method to combine the four individual fouling mechanisms. Explicit equations were derived to relate the pressure to the time during constant flow operation and the vol-

Table 1. Solutions of Eq. 4 for different n values (Hermia's fouling models).

Fouling mechanisms	n	Fouling models	Linear forms
Cake filtration	0	$J = \frac{J_0}{(1 + J_0^2 kt)^{0.5}}$	$\frac{1}{J^2} = \frac{1}{J_0^2} + kt$
Intermediate blockage	1	$J = \frac{J_0}{(1 + J_0 kt)}$	$\frac{1}{J} = \frac{1}{J_0} + kt$
Standard blockage	1.5	$J = \frac{J_0}{(1 + J_0^{0.5} kt)^2}$	$\frac{1}{J^{0.5}} = \frac{1}{J_0^{0.5}} + kt$
Complete blockage	2	$J = J_0 \exp(-kt)$	$\ln\left(\frac{1}{J}\right) = \ln\left(\frac{1}{J_0}\right) + kt$

ume to the time during constant pressure operation. All the models have two fitted parameters and are reduced to individual models in the absence of second fouling mechanisms. A summary of constant pressure combined fouling models is provided in Table 2.

EXPERIMENTAL

Materials

Commercial isotactic polypropylene (i-PP, EPD60R, MFI = 0.35 g/10min, Arak Petrochemical Co.) as polymer, mineral oil (MO, Acros Organics) as diluent, Irganox (1010, Ciba Co.) as heat stabilizer and acetone (Merck) as oil extractor were used for membrane fabrication. Bovine serum albumin (BSA, Sigma-Aldrich, M_w = 66.5kDa) and collagen (Sigma-Aldrich, M_w = 139kDa) proteins were used as model proteins. Phosphate buffered saline (PBS, pH 7.4) and HCl aqueous solution (pH 3) were used to prepare the BSA and collagen proteins solutions, respectively. PBS was prepared by adding a certain amount of buffer salts to deionized water. All materials were used as received without further treatment.

Membrane fabrication

The PP microporous membrane was fabricated via TIPS method. 24 g iPP polymer granule and 1 g Irganox 1010 were added to the 75 g MO. The mixture was melt blended at 170°C and 300 rpm in a sealed glass vessel kept in a silicon oil bath. The solution was then allowed to degas for 30 min and to cast on a preheated

glass plate using a doctor blade with the film thickness of 300 µm. The plate was immediately quenched in the water bath of 30°C to induce phase separation. The membrane was then immersed in acetone for 24 h to extract its diluent. Finally, membranes were dried at room temperature for 2 h [40].

Membrane morphology observation and pore size measurement

The morphology of the fabricated membrane was observed by a scanning electron microscope (SEM) (VEGA3, TESCAN). To observe the membrane cross-section, membrane sample was immersed in liquid nitrogen and then was broken, carefully. All samples were coated with a thin layer of gold by sputtering before observation to become conductive.

Average surface and internal pore sizes of fabricated membrane were determined from SEM images and image analysis software ImageJ.

Pure water flux

Pure water flux of membranes was determined by an in-house fabricated dead-end filtration system having 5 cm² of membrane area at 0.75, 1.5 and 2 bar. To do this, membrane sample was pre-wetted by ethanol with immersing the membrane in ethanol for 30 min. Then the membrane was set in the filtration system. To minimize the compaction effect on the membrane flux, the pre-wetted membrane was compacted for 90 min and after reaching steady state, water flux was calculated by the following equation:

Table 2. Combined fouling models at constant pressure.

Fouling mechanisms	Fouling models	Fitted parameters
Cake filtration-complete blockage (CFCBM)	$V = \frac{J_0}{K_b} (1 - \exp(-\frac{k_b}{k_c J_0^2} (\sqrt{1 + 2k_c J_0^2 t} - 1)))$	k_b (min ⁻¹), k_c (min/m ²)
Cake filtration-intermediate blockage (CFIBM)	$V = \frac{1}{k_i} \ln(1 + \frac{k_i}{k_c J_0} (\sqrt{1 + 2k_c J_0^2 t} - 1))$	k_i (m ⁻¹), k_c (min/m ²)
Cake filtration-standard blockage (CFSBM)	$V = \frac{2}{k_s} \left(\beta \cos\left(\frac{2\pi}{3} - \frac{1}{3} \arccos(\alpha)\right) + \frac{1}{3} \right)$ $\alpha = \frac{8}{27\beta^3} + \frac{4k_s}{3\beta^3 k_c J_0} - \frac{4k_s^2 t}{3\beta^3 k_c}$ $\beta = \sqrt{\frac{4}{9} + \frac{4k_s}{3k_c J_0} - \frac{2k_s^2 t}{3k_c}}$	k_s (m ⁻¹), k_c (min/m ²)

$$J_p = \frac{V}{At} \quad (5)$$

where J_p is the pure water flux, V is the volume of collected water (l), A is the membrane area (m^2) and t is the time (h).

Protein solution preparation

In order to investigate the protein fouling of polypropylene microfiltration membrane, BSA and collagen proteins solutions were prepared and filtered through membrane at three different operational pressures. To prepare BSA protein solution, 1g of BSA protein powder was dissolved in 1L of PBS solution (pH 7.4).

In order to prepare a collagen protein solution, a similar method mentioned in our previous published work [41] was carried out, in which 1 gr of collagen protein powder was dissolved in 1L of PBS solution (pH 7.4). In order to prevent proteins denaturation, proteins solutions were prepared and kept at 0°C using the ice bath.

Protein fouling tests through dead-end filtration experiments

In order to study the effect of operational pressure and foulant type, microfiltration processes of protein solutions with the prepared microporous membrane were conducted using an in-house manufactured dead-end filtration system. At each filtration process, the transmembrane pressure was set at desired pressure, manually. In order to eliminate the membrane compaction effect on the membrane flux decline at each filtration process, the membranes were compacted with pure water for 90 min before protein solution filtration. After reaching steady state condition, the pure water flux was measured at each operational pressure. Then the protein solution was filtered for about 120 min at each filtration process and flux decline was depicted versus time during filtration. After about 120 min protein solution filtration, the membrane cell was again connected to the pure water filtration system and pure water flux after fouling (J_1) was measured using Eq. 5. Then the cake layer on the membrane was gently removed mechanically by a sponge and the membrane was immersed in deionized water for 1h. Finally, the membrane was held in the holder and connected to the pure water filtration system and pure water flux after

rinsing (J_2) was measured using Eq. 5. With J_p , J_1 and J_2 on hand, we can determine the fouling ratios and flux recovery [33, 34]. The total fouling ratio (TFR) of a membrane is defined as follows:

$$TFR = \left(\frac{J_p - J_1}{J_p} \right) \times 100 \quad (6)$$

TFR is the sum of reversible fouling ratio (RFR) and irreversible fouling ratio (IFR), which

can be defined by the following equations:

$$RFR = \left(\frac{J_2 - J_1}{J_p} \right) \times 100 \quad (7)$$

$$IFR = \left(\frac{J_p - J_2}{J_p} \right) \times 100 \quad (8)$$

Finally, the flux recovery (FR) can be calculated as follow:

$$FR = \left(\frac{J_2}{J_p} \right) \times 100 \quad (9)$$

The flux recovery is an index of antifouling property of membranes.

Protein retention

The retention percentage of BSA and collagen proteins by polypropylene microfiltration membrane was calculated by the following equation:

$$R(\%) = \left(1 - \frac{C_p}{C_f} \right) \times 100 \quad (10)$$

where C_p and C_f are the concentrations of proteins in permeate and feed, respectively. The concentrations of BSA and collagen proteins in the feed and permeate were estimated with a UV-VIS spectrophotometer (Agilent-HP 8452A) at wavelengths of 278 and 540 nm, respectively.

Analysis of fouling mechanism

In order to identify the fouling mechanism during microfiltration of proteins solutions by PP membrane, Hermia's fouling models as well as combined fouling models presented in Table 1 and Table 2, respectively, were fitted to the experimental data of each filtration process, using the least square method. The best fit

was determined by minimizing the sum of squared residuals, where the residual is equal to the difference between a data point and the model prediction. All the calculations were carried out by curve fitting tool of MATLAB software. This tool of MATLAB software enables to fit any equation with different constants to experimental data with high accuracy and reliability.

RESULTS AND DISCUSSION

Membrane morphology observation

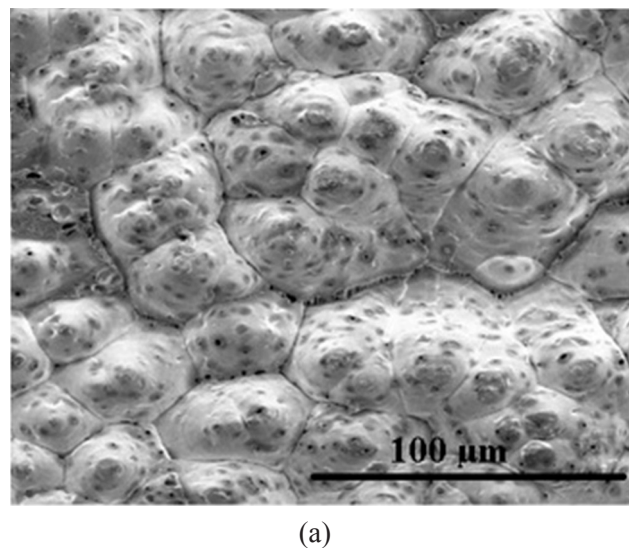
SEM images of the surface and cross-section of the fabricated membrane at different magnifications are shown in Figure 1. From the SEM images of cross-

section it can be seen that the membrane has sponge like porosity and symmetric structure.

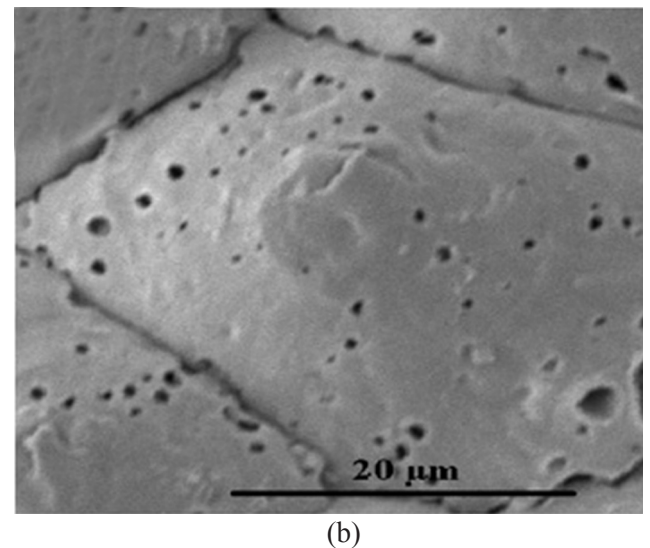
Fabricated membrane approximately has the average surface pore size of $0.256 \pm 0.136 \mu\text{m}$ and internal pore size of $0.667 \pm 0.169 \mu\text{m}$ which were measured by ImageJ software. It has been reported that the microfiltration membranes have the pore size of $0.1\text{-}10 \mu\text{m}$ [1]. So, the obtained results confirm the microporous structure of the fabricated PP membrane.

Pure water flux

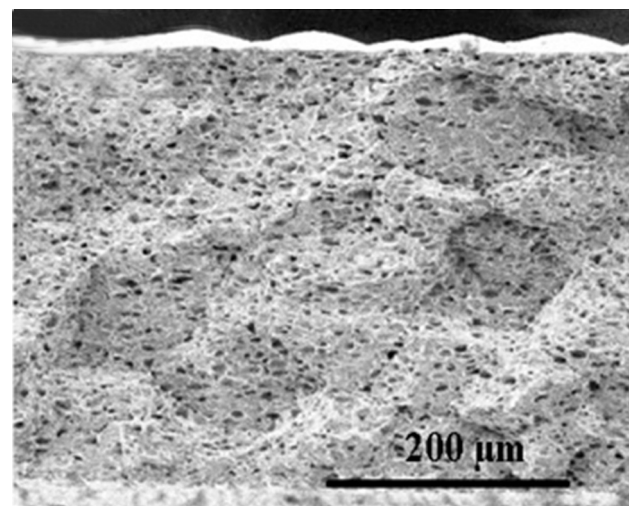
Pure water flux of the fabricated PPMM was measured at each operational pressure and the results are presented in Figure 2. It can be seen that increasing the trans-membrane pressure leads to pure water flux increment due to the higher driving force across the



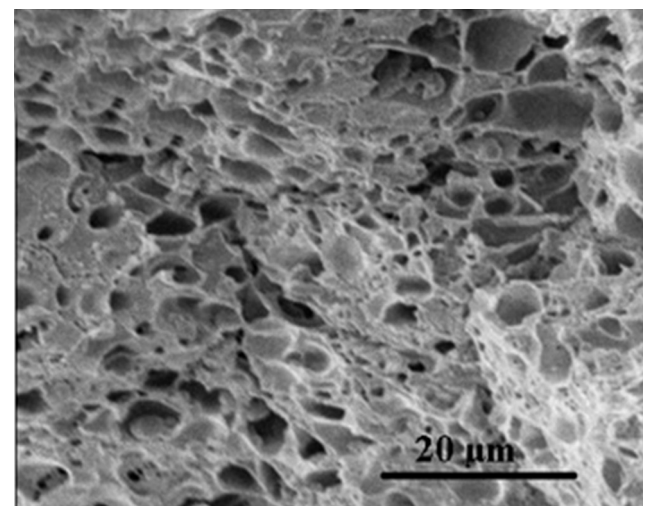
(a)



(b)



(c)



(d)

Figure 1. SEM images of fabricated PP microporous membrane. (a) Surface (1000 \times), (b) surface (enlarged, 5000 \times), (c) cross-section (500 \times), and (d) cross-section (enlarged, 4000 \times).

membrane. The obtained results were in good agreement with the finding reported by Nandi et al. [42].

Protein fouling tests through dead-end filtration experiments

Permeate flux decline versus time during BSA and collagen solutions microfiltration at different operational pressures is presented in Figure 3. According to Figure 3, it can be seen that for all filtration processes, permeate flux reduces constantly until it reaches a uniform rate known as steady-state. Permeate flux decline during filtration process occurs due to concentration polarization and fouling phenomenon [1]. Concentration polarization results in higher solute concentration in the region close to the membrane surface than the bulk feed stream, which is caused due to the diffusive flow of solute back to the bulk feed [43]. Although the concentration polarization leads to permeate flux decline, it is different from fouling and is not considered as fouling, because once the filtration process is stopped, concentration polarization disappears [1, 44]. According to Figure 3, in the case of BSA solution filtration (Figure 3 (a)) as well as collagen solution filtration (Figure 3 (b)), it can be seen that the permeate flux decline becomes more severe with increasing operational pressure. So, the permeate flux decreases from 11.265 to 3.805 L/m²h at 0.75 bar, from 24.450 to 8.363 L/m²h at 1.5 bar and from 35.45 to 12.763 L/m²h at 2 bar for BSA solution filtrations. In the case of collagen solution filtration, the permeate flux decreases from 8.889 to 3.456 L/m²h at 0.75 bar, from 20.326 to 4.796 L/m²h at 1.5 bar, and from 29.326 to 6.796 L/m²h at 2 bar. It is due to the higher permeate flux according to higher driving force across the membrane, which results in severe concentration polarization.

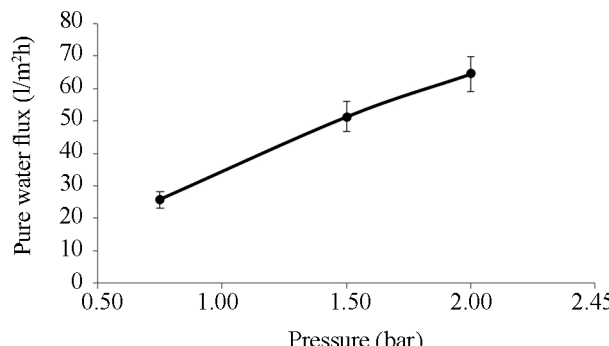


Figure 2. Pure water flux of fabricated PP microporous membrane at different operational pressure.

Higher permeate flux leads to higher transportation of protein macromolecules to the membrane surface and higher accumulation of these macromolecules near the membrane surface at the certain filtration time.

Moreover, it can be seen that the flux decline during collagen solution filtration is much more severe than that of BSA solution filtration at the same operational pressure and becomes sharper by increasing the operational pressure. Therefore, permeate fluxes at the end of the filtration processes of BSA and collagen solutions are 3.805 and 3.456 L/m²h at 0.75 bar, 8.383 and 4.796 L/m²h at 1.5 bar, and 12.763 and 6.796 L/m²h at 2 bar, respectively. This may be attributed to the difference in the sizes of the BSA and collagen proteins' molecules. BSA is a globular protein with 66 kDa and

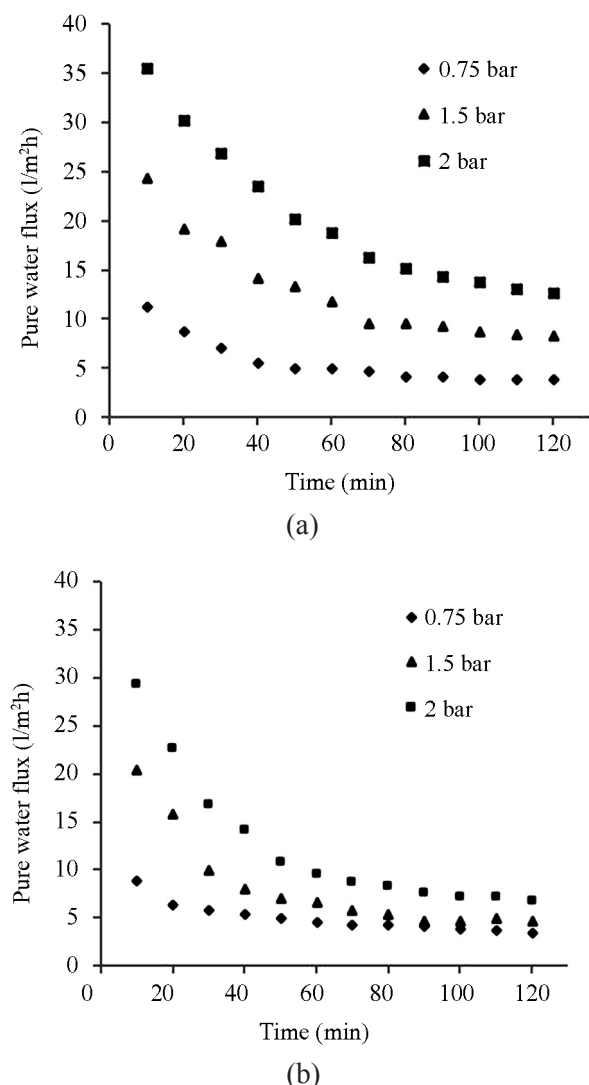


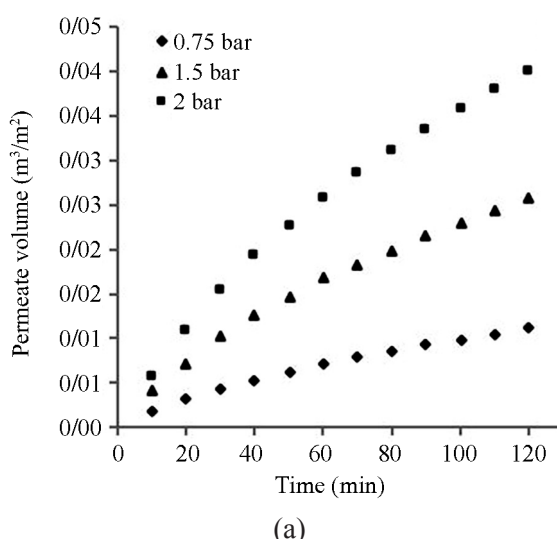
Figure 3. Permeate flux versus time at different operational pressures. (a) BSA solution filtrations, and (b) Collagen solution filtrations.

0.014 μm of average molecular weight and normal diameter, respectively [45]. Collagen, however, is a filamentous protein with 139 kDa, 0.3 μm and 1.5 nm of average molecular weight, length and diameter, respectively. Comparison of the molecular weight of the BSA and collagen proteins shows that the concentration polarization can be much more severe in the case of collagen solution filtration due to the lower diffusion coefficient and consequently lower mass transfer coefficient of collagen protein [23]. Therefore, diffusion across the membrane cross-section and back diffusion into the feed bulk of collagen macromolecules would be very low, which consequently results in higher accumulation of collagen macromolecules in the vicinity of the membrane surface and higher concentration polarization.

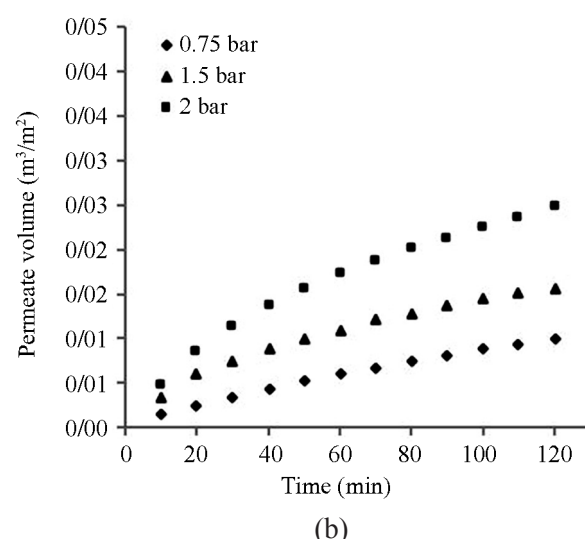
Permeate volumes versus time at different operational pressures for BSA and collagen solutions filtration are depicted at Figure 4. It can be seen that, for both protein solution filtrations, increasing operational pressure results in higher feed filtration in a certain filtration period. Moreover, comparing Figs. 4 (a) and (b) reveals that at the same operational pressure, the amount of the filtrated BSA solution is higher than that of the collagen solution at the end of each filtration period. The difference in the amount of permeate volumes becomes more severe by increasing the operational pressure. It could also be attributed to the aforementioned concentration polarization phenomenon, as

explained in the previous paragraph.

Based on the measured values of J_p , J_1 , J_2 and data obtained from Eqs. 6-9 for each filtration process, fouling ratios and flux recoveries were calculated. The calculation results are presented in Figure 5 for BSA and collagen ollagen solutions filtrations. The results show that, in the case of BSA solution filtration, TFR decreases by decreasing the operational pressure. The obtained results show that the TFR is 68.72, 61.56 and 49.48% at 2, 1.5 and 0.75 bar, respectively. Moreover, it can be seen that the RFR is very low for BSA solution filtration at each operational pressure and decreases slightly by increasing pressure. RFR for BSA solution filtration is about 11.20, 13.84 and 15.46% at 2, 1.5 and 0.75 bar, respectively. The IFR is 57.52, 47.72, and 34.02% at 2, 1.5 and 0.75 bar, respectively. It is clear that, increasing the operational pressure results in higher IFR. It could be attributed to the more penetration of macromolecules into the membrane pores due to the high driving force exerted by increased trans-membrane pressure. As it has been said earlier, TFR is the sum of RFR and IFR. Therefore, it is obvious that the higher portion of TFR in BSA solution filtration belongs to IFR in all operational pressures, which results in lower flux recovery of the membrane. The FR for BSA solution filtration is 42.48, 52.28 and 65.97% at 2, 1.5 and 0.75 bar, respectively. It is also obvious that the flux recovery increases with decreasing the operational pressure.



(a)



(b)

Figure 4. Permeate volume versus time at different operational pressures. (a) BSA solution filtrations, and (b) Collagen solution filtrations.

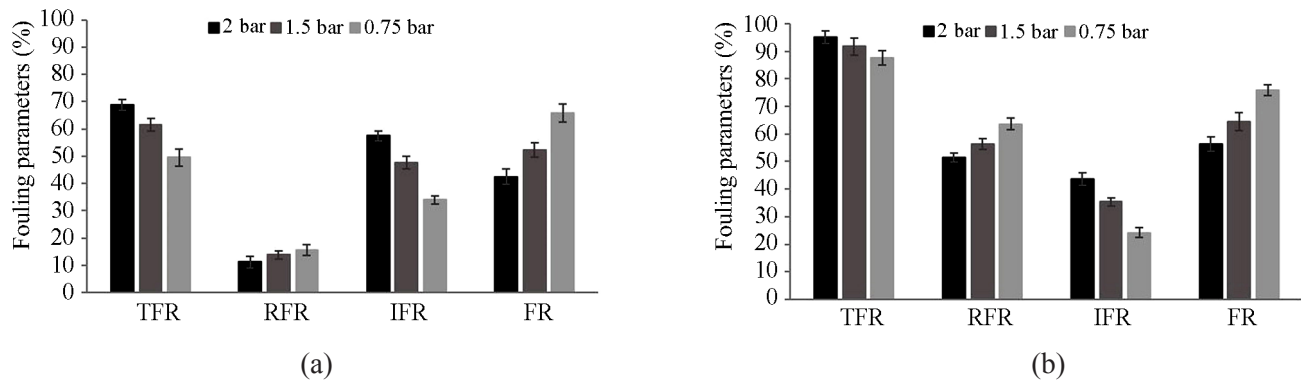


Figure 5. Fouling ratios and flux recovery at different operational pressures of 0.75, 1.5, and 2 bar. (a) BSA solution filtrations, and (b) Collagen solution filtrations. TFR: Total fouling ratio, RFR: Reversible fouling ratio, IFR: Irreversible fouling ratio, and FR: Flux recovery.

In the case of collagen solution filtration, the TFR is very high for all operational pressure ranges and increases slightly as pressure is increased. TFR is 95.11 at 2 bar, 91.75 and 87.68 at 1.5 and 0.75 bar, respectively. Comparing RFR and IFR for collagen solution filtrations shows that, unlike the BSA solution filtrations, the high portion of the TFR belongs to RFR. So, the FR of membrane for collagen solution filtration is higher than the BSA solution filtration at the same operational pressure. The FR value for collagen solution filtration is 56.32, 64.53 and 75.83% at 2, 1.5 and 0.75 bar, respectively. Similar to the BSA solution filtrations, in collagen solution filtration processes FR decreases with increasing the pressure. The results of fouling ratios and flux recoveries for BSA and collagen solutions filtrations show that the foulant size and structure are key parameters in protein filtration processes.

As has been said earlier, it can be speculated that globular structure of BSA protein would result in easy penetration of macromolecule into the membrane pores and entrapment inside the microporous structure of the membrane, which consequently results in severe internal fouling. Lower FR of the membranes after cleaning with distilled water in BSA solution filtration (a) also supports this speculation. Collagen molecules with larger size and unique fibrous structure, however, are retained at the membrane surface more readily than BSA molecules and a few number of collagen molecules can enter the membrane pores and result in internal fouling. Moreover, the retained molecules of collagen accumulate on each other and

act as a secondary barrier against the other collagen molecules that reach the membrane surface. Therefore, higher FR of membrane in collagen solution filtration processes compared to BSA solution filtration can be justified with the different size and structure of two selected proteins. In comparison with BSA protein, the higher TFR of collagen solution filtration can be related to the size and structure of proteins. Collagen macromolecules cannot enter into the membrane pores and hence collagen molecules are retained with membrane and accumulate near the membrane surface, which helps cake formation and consequently higher TFR.

Protein retention

The retentions of BSA and collagen proteins by PPMM for each filtration process were evaluated by measuring the concentration of proteins in the feed and permeate streams and the results were summarized in Table 3. The results show that, for both protein solutions filtration, operational pressure does not have considerable effect on retention values, and retention values decrease very slightly by increasing the operational pressure, which can be attributed to the higher driving force exerted on the protein macromolecules at higher pressures. Moreover, it can be seen that the retention of collagen is higher than the BSA. It must be due to the difference in sizes as well as the structures of both proteins. As has been mentioned in the previous section, collagen macromolecules with special fibrous structure, higher molecular weight, and bigger size cannot pass through the membrane cross-section

as easily as BSA macromolecules with globular structure, lower molecular weight, and smaller size. Therefore the collagen removal efficiency of the membrane will be higher than that of BSA.

It is interesting to note that, although the sizes of BSA and collagen macromolecules appear to be smaller than the membrane pore size; measured by SEM images; the pore tortuosity and contraction across the cross-section of the membrane help to capture the BSA and collagen macromolecules, which results in high protein retention of microporous membrane [10].

Analysis of fouling mechanism

Hermia's models

Hermia's fouling models were fitted to the experimental data by using MATLAB software of each filtration process in order to find the best fouling model describing membrane fouling during microfiltration of BSA and collagen solutions. The results of fitting the fouling models to experimental data of BSA and collagen solutions are presented in Tables 4 and 5, respectively. For each filtration process, the model with higher correlation coefficient (R^2) has been selected as the best model describing the fouling mechanism. According to the data shown in Tables 4 and 5, it can be seen that the experimental data at 0.75 bar for BSA and collagen solutions filtrations are well fitted with cake filtration model since the R^2 values of this model for BSA and collagen solutions, equal with 0.9758 and 0.9865, respectively, are higher than the R^2 values of other mechanism consisting of intermediate, standard and complete blockage models. Increasing the operational pressure from 0.75 to 1.5 bar leads to fouling mechanism change from cake filtration model to intermediate blocking model for both BSA and collagen solutions filtrations. R^2 values of intermediate blockage model are equal to 0.9824 and 0.9736 for BSA and collagen solutions filtrations, respectively at 1.5 bar. For each

Table 3. Retention performance of PP microporous membrane in the filtration processes of BSA and collagen proteins solutions.

BSA solution filtration	Retention (%)	Collagen solution filtration	Retention (%)
0.75 bar	83.34 ± 0.43	0.75 bar	97.55 ± 0.44
1.5 bar	81.45 ± 0.66	1.5 bar	96.11 ± 0.56
2 bar	78.93 ± 0.48	2 bar	94.63 ± 0.54

Table 4. Values of k and correlation coefficient (R^2) for BSA solution filtrations at different operational pressures based on the Hermia's models.

P(bar)	Models	R^2	k
0.75	n = 0	0.9865	0.0006584
	n = 1	0.9542	0.002113
	n = 1.5	0.9139	0.002535
	n = 2	0.8609	0.01162
1.5	n = 0	0.9770	0.000115
	n = 1	0.9824	0.0008598
	n = 1.5	0.9558	0.001601
	n = 2	0.9344	0.01149
2	n = 0	0.9765	0.00004383
	n = 1	0.9956	0.0005066
	n = 1.5	0.9890	0.00118
	n = 2	0.9695	0.01066

protein solution filtration process at 2 bar, intermediate blockage model still shows better fitting than other models with R^2 values of 0.9956 and 0.9901 for BSA and collagen solutions filtrations, respectively. It can be concluded that increasing the operation pressure changes the cake filtration mechanism of fouling into the pore blocking mechanism for both proteins with different sizes and structures. It may be the key reason of lower flux recovery at higher operational pressures, discussed in the previous section.

Experimental flux decline data versus time and predicted flux decline data using Hermia's fouling models for filtration processes of BSA and collagen solutions are shown in Figure 6.

Combined models

Combined models were fitted to the experimental data of BSA and collagen solutions filtrations at different

Table 5. Values of k and correlation coefficient (R^2) for collagen solution filtrations at different operational pressures based on the Hermia's models.

P(bar)	Models	R^2	k
0.75	n=0	0.9758	0.0006607
	n=1	0.9308	0.001722
	n=1.5	0.9000	0.001908
	n=2	0.8659	0.008306
1.5	n=0	0.9172	0.0002961
	n=1	0.9736	0.002057
	n=1.5	0.9443	0.003243
	n=2	0.8799	0.01875
2	n=0	0.9430	0.0001296
	n=1	0.9901	0.001244
	n=1.5	0.9734	0.002412
	n=2	0.9264	0.01745

operational pressures by using MATLAB software. According to Table 2, each combined model has three unknown parameters that must be calculated by fitting the models to experimental data. J_0 is one of the three unknown parameters at each combined model, which is defined as permeate flux at the beginning of the filtration (permeate flux at $t = 0$). J_0 cannot be measured experimentally and according to the Bolton et al. [27], it is a physical characteristic of a membrane. Hence, although we cannot measure the J_0 , but we know its reasonable range. For example, fabricated membrane in this study via TIPS method cannot have the J_0 higher than $100 \text{ L/m}^2\text{h}$ at each filtration pressure. So, the amount obtained for J_0 from the fitting of combined models to experimental data must be proportional to pure water flux of the membrane, which is presented in Figure 2. The results of fitting of the combined models with the experimental data of BSA and collagen solutions filtrations are presented in Tables 6 and 7, respectively. As shown in Table 6, at each operational pressure of BSA solution filtration, R^2 value of each combined model is very near the unity. However, the obtained J_0 values for CFCBM are 12600, 12996 and $14094 \text{ L/m}^2\text{h}$ at 0.75, 1.5 and 2 bar, respectively, which are unreasonable J_0 values for fabricated membranes. Moreover, the obtained J_0 values from CFIBM model are equal with 3535.8, 4674 and $5221.8 \text{ L/m}^2\text{h}$ at 0.75, 1.5 and 2 bar, respectively, which are also unreasonable values for fabricated membrane. In the case of the R^2 value close to unity for the fitting of the experimental data with CFSBM model, it can be seen that at each operational pressure, the obtained J_0 values are reasonable. The obtained J_0 values for CFSBM of BSA solution filtration are 13.97, 29.03 and $41.01 \text{ L}/$

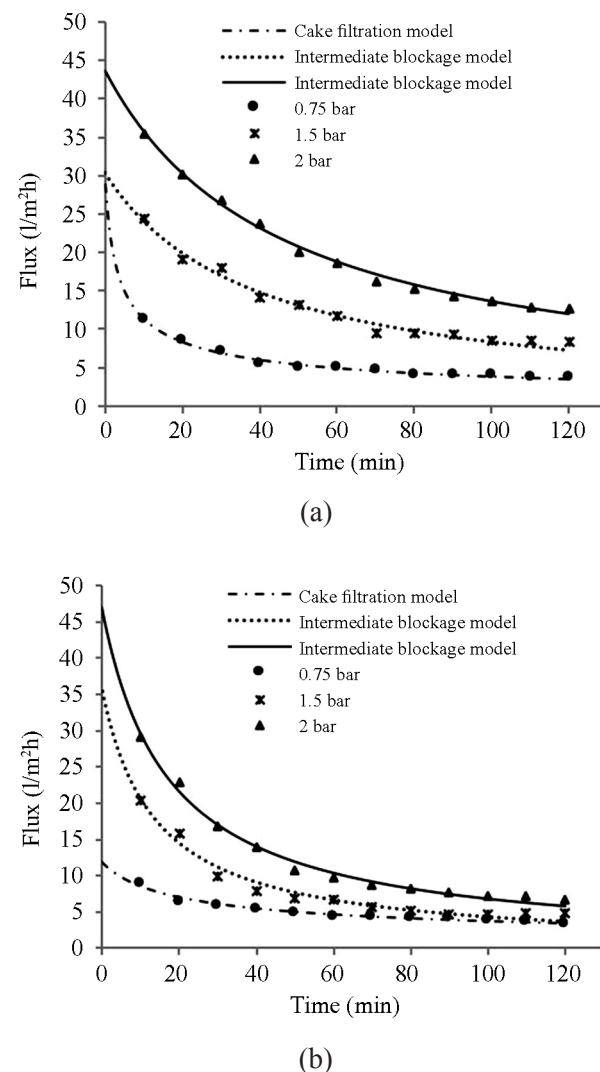


Figure 6. Experimental flux decline data in company with predicted flux decline data using Hermia's fouling models. (a) BSA solution filtrations, and (b) Collagen solution filtration.

m^2h at 0.75, 1.5 and 2 bar, respectively. Therefore, it can be seen that the suggested fouling mechanism for BSA solution filtration at each operational pressure is

Table 6. Values of correlation coefficient (R^2), J_0 and k for BSA solution filtration at different operating pressures based on the combined models. CFCBM: cake filtration-complete blockage model, CFIBM: cake filtration-intermediate blockage model, and cake filtration- standard blockage model.

P (bar)	Models	R^2	$J_0 (\text{L/m}^2\text{h})$	Fitted parameters
0.75	CFCB	0.9996	10452	$k_b = 0.0008798 (\text{min}^{-1})$, $k_c = 1.003 (\text{min}/\text{m}^2)$
	CFIB	0.9941	2976.6	$k_i = 13.95 (\text{m}^{-1})$, $k_c = 3.006 (\text{min}/\text{m}^2)$
	CFSB	0.9997	9.204	$k_s = 15.73 (\text{m}^{-1})$, $k_c = 10^6 (\text{min}/\text{m}^2)$
1.5	CFCB	0.9994	13278	$k_b = 5.273 (\text{min}^{-1})$, $k_c = 2.467 (\text{min}/\text{m}^2)$
	CFIB	0.9994	4811.4	$k_i = 33.39 (\text{m}^{-1})$, $k_c = 15.47 (\text{min}/\text{m}^2)$
	CFSB	0.9992	38.03	$k_s = 73.13 (\text{m}^{-1})$, $k_c = 5 \times 10^5 (\text{min}/\text{m}^2)$
2	CFCB	0.9995	13932	$k_b = 3.916 (\text{min}^{-1})$, $k_c = 1.202 (\text{min}/\text{m}^2)$
	CFIB	0.9995	5211.6	$k_i = 25.87 (\text{m}^{-1})$, $k_c = 6.364 (\text{min}/\text{m}^2)$
	CFSB	0.9993	41.42	$k_s = 50 (\text{m}^{-1})$, $k_c = 10^5 (\text{min}/\text{m}^2)$

combination of cake filtration and standard blocking (CFSBM) models.

From the results reported in Table 7, it can be seen that for collagen solution filtration, at each filtration pressure the R^2 values of CFCBM, CFIBM and CFSBM are almost 1. However, the obtained J_o from CFCBM and CFIBM is very high and unreasonable for each filtration process. Therefore, it can be concluded that CFSBM is the most reasonable model that can describe the flux decline mechanism during microfiltration of collagen solution. The obtained J_o values from the CFSBM model in the collagen solution filtration process are 9.204, 38.03 and 42.18 L/m²h at 0.75, 1.5, and 2 bar operational pressures, respectively. Combined cake filtration-standard blockage model relates the fouling mechanism to combined effect of cake formation and internal pore blocking. With respect to the surface pore size of the fabricated membrane and the sizes of BSA and collagen macromolecules it is expected that some of the molecules can enter into the pores and trap in microporous structure of membrane and result in internal blocking. Therefore, CFSBM fouling mechanism can be considered as the most reasonable mechanism for flux decline during BSA and collagen solution filtration.

Experimental filtrate volume data versus time and predicted filtrate volume data using combined fouling models for filtration processes of BSA and collagen solutions are presented in Figure 7. It can be seen that, combined fouling models show very good agreement with experimental data. This finding has also been confirmed by several published works [27, 33-35].

The contributions of standard blockage and cake filtration to combined CFSBM model are also eval-

uated from the values of k_c and k_s . The values of $k_c J_o$ and k_s have units of m⁻¹ and will be of similar magnitude when their contributions to the combined model of CFSBM are similar [27]. The values of $k_c J_o / k_s$ ratio for each filtration process were calculated and are presented in Table 8. As can be seen in Table 8, operational pressure and protein type have considerable effect on the $k_c J_o / k_s$ values. For BSA as well as collagen solutions filtrations, $k_c J_o / k_s$ value decreases by increasing the operational pressure. So that, by increasing the operational pressure from 0.75 to 2 bar, $k_c J_o / k_s$ decreases from 5.87 to 0.28 and from 9.75 to 1.38 for BSA and collagen solutions filtrations, respectively, which means that the contribution of standard blockage mechanism to the fouling of the membrane has increased by increasing the operational pressure. Moreover, the results of Table 8 show that, at the same operational pressure, $k_c J_o / k_s$ values for collagen solution filtrations are higher than that of BSA solution filtrations, therefore it can be concluded that the contribution of cake filtration mechanism to membrane fouling in collagen solution filtrations is higher than that of BSA solution filtrations. It is clear that an increment in the contribution of the cake filtration mechanism to membrane fouling leads to higher flux recovery of the membrane. Therefore, the higher flux recovery of the membrane in collagen solution filtration processes can be justified by the higher values of $k_c J_o / k_s$, too. It can be seen that the obtained results of combined models are in very good agreement with the experimental data of previous sections, which confirms the ability of the new combined models to prediction of membrane fouling mechanisms.

Table 7. Values of correlation coefficient (R^2), J_o and k for collagen solution filtration at different operating pressures based on the combined models. CFCBM: cake filtration-complete blockage model, CFIBM: cake filtration-intermediate blockage model, and cake filtration- standard blockage model.

P (bar)	Models	R^2	J_o (L/m ² h)	Fitted parameters
0.75	CFCB	0.9996	10452	$k_b = 0.0008798$ (min ⁻¹), $k_c = 1.003$ (min/m ²)
	CFIB	0.9941	2976.6	$k_i = 13.95$ (m ⁻¹), $k_c = 3.006$ (min/m ²)
	CFSB	0.9997	9.204	$k_s = 15.73$ (m ⁻¹), $k_c = 10^6$ (min/m ²)
1.5	CFCB	0.9994	13278	$k_b = 5.273$ (min ⁻¹), $k_c = 2.467$ (min/m ²)
	CFIB	0.9994	4811.4	$k_i = 33.39$ (m ⁻¹), $k_c = 15.47$ (min/m ²)
	CFSB	0.9992	38.03	$k_s = 73.13$ (m ⁻¹), $k_c = 5 \times 10^5$ (min/m ²)
2	CFCB	0.9995	13932	$k_b = 3.916$ (min ⁻¹), $k_c = 1.202$ (min/m ²)
	CFIB	0.9995	5211.6	$k_i = 25.87$ (m ⁻¹), $k_c = 6.364$ (min/m ²)
	CFSB	0.9993	41.42	$k_s = 50$ (m ⁻¹), $k_c = 10^5$ (min/m ²)

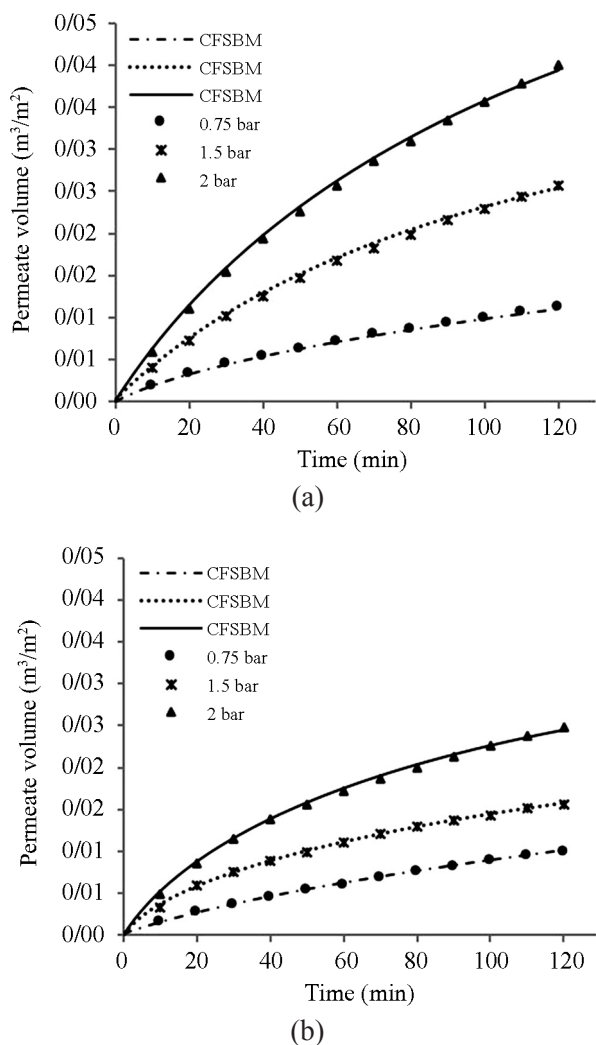


Figure 7. Experimental permeate volume data in company with predicted permeate volume data using combined fouling models. (a) BSA solution filtrations, and (b) Collagen solution filtration.

CONCLUSION

Polypropylene microporous membrane with special structure for protein separation and purification was fabricated via thermally induced phase separation method. Microporous structure of the membrane was confirmed by SEM images and ImageJ software. BSA and collagen solutions as two types of proteins with

Table 8. Contributions of cake filtration and standard blockage to membrane fouling at each filtration process.

Operational pressure (bar)	$k_c J_o / k_s$ BSA solution filtrations	$k_c J_o / k_s$ Collagen solution filtrations
0.75	5.87	9.75
1.5	1.58	4.33
2	0.28	1.38

different sizes, molecular weights, and structures were filtered by fabricated microporous membrane at different operational pressures and the effect of protein type and operational pressure on membrane fouling as well as membrane filtration performance were evaluated. The obtained results showed that the higher amount of BSA solution was filtered by the membrane than the collagen solution at the same filtration period and the flux decline was more severe in collagen solution filtration than BSA solution filtration which was attributed to the different sizes and structures of the aforementioned proteins. Fouling analysis of the membrane showed that, however the flux decline in collagen solution filtrations was severe, the reversible fouling ratio and consequently flux recovery of the membrane were high in collagen solution filtration processes. Moreover, the high retention values, especially in collagen solution filtrations, showed that the protein removal efficiency of the fabricated membrane with microporous structure was very high due to the pore tortuosity and contraction across the cross-section of the membrane.

In addition, fouling mechanisms of membrane at each filtration process were evaluated by well-known Hermia's fouling models and newly presented combined fouling models. The results showed that the operational pressure and foulant type were affecting fouling mechanism of membrane considerably. Moreover, it was concluded that combined models by relating the membrane fouling to combination of two fouling mechanisms had potential ability in prediction of fouling mechanisms during filtration processes. This ability was confirmed by the good agreement of predicted data with experimentally obtained permeate volume results.

REFERENCES

- Mulder M (1996) Basic principles of membrane technology Kluwer Academic Publishers, Second ed.,
- Ulbricht M (2006) Advanced functional polymer membranes. *Polymer* 47: 2217-2262
- Hilal N, Ogunbiyi OO, Milles JN, Nigmatullin R (2005) Methods employed for control of fouling

- in MF and UF membranes: A comprehensive review. *Separ Sci Tech* 40: 1957-2005
4. Xu Q, Yang J, Dai J, Yang Y, Chen X, Wang Y (2013) Hydrophilization of porous polypropylene membranes by atomic layer deposition of TiO₂ for simultaneously improved permeability and selectivity. *J Membrane Sci* 448: 215-222
 5. Yu H-Y, Xu Z-K, Lei H, Hu M-X, Yang Q (2007) Photoinduced graft polymerization of acrylamide on polypropylene microporous membranes for the improvement of antifouling characteristics in a submerged membrane-bioreactor. *Separ Purif Tech* 53: 119-125
 6. Hu M-X, Yang Q, Xu Z-K (2006) Enhancing the hydrophilicity of polypropylene microporous membranes by the grafting of 2-hydroxyethyl methacrylate via a synergistic effect of photoinitiators. *J Membrane Sci* 285: 196-205
 7. van de Witte P, Dijkstra PJ, van den Berg JWA, Feijen J (1996) Phase separation processes in polymer solutions in relation to membrane formation. *J Membrane Sci* 117: 1-31
 8. Strathmann H, Kock K (1977) The formation mechanism of phase inversion membranes. *Desalination* 21: 241-255
 9. K Pubby A, S H Rizvi S, Maria Sastre A (2009) Handbook of membrane separations: Chemical, pharmaceutical, food and biotechnological applications, CRC Press
 10. Zhu X, Loo H-E, Bai R (2013) A novel membrane showing both hydrophilic and oleophobic surface properties and its non-fouling performances for potential water treatment applications. *J Membrane Sci* 436: 47-56
 11. Xia B, Zhang G, Zhang F (2003) Bilirubin removal by Cibacron Blue F3GA attached nylon-based hydrophilic affinity membrane. *J Membrane Sci* 226: 9-20
 12. Bottino A, Capannelli G, Turchini A, Della Valle P, Trevisan M (2002) Integrated membrane processes for the concentration of tomato juice. *Desalination* 148: 73-77
 13. Morão A, Brites Alves AM, Cardoso JP (2001) Ultrafiltration of demethylchlortetracycline industrial fermentation broths. *Separ Purif Technol* 22-23: 459-466
 14. Alves AMB, Morão A, Cardoso JP (2002) Isolation of antibiotics from industrial fermentation broths using membrane technology. *Desalination* 148: 181-186
 15. Kelly ST, Zydny AL (1995) Mechanisms for BSA fouling during microfiltration. *J Membrane Sci* 107: 115-127
 16. Shen J-n, Li D-d, Jiang F-y, Qiu J-h, Gao C-j (2009) Purification and concentration of collagen by charged ultrafiltration membrane of hydrophilic polyacrylonitrile blend. *Separ Purif Technol* 66: 257-262
 17. Yan M-G, Liu L-Q, Tang Z-Q, Huang L, Li W, Zhou J, Gu J-S, Wei X-W, Yu H-Y (2008) Plasma surface modification of polypropylene microfiltration membranes and fouling by BSA dispersion. *Chem Eng J* 145: 218-224
 18. Wang Y-N, Tang CY (2011) Protein fouling of nanofiltration, reverse osmosis, and ultrafiltration membranes—The role of hydrodynamic conditions, solution chemistry, and membrane properties. *J Membrane Sci* 376: 275-282
 19. Voswinkel L, Kulozik U (2014) Fractionation of all major and minor whey proteins with radial flow membrane adsorption chromatography at lab and pilot scale. *Int Dairy J* 39: 209-214
 20. Schoenbeck I, Graf AM, Leuthold M, Pastor A, Beutel S, Schepers T (2013) Purification of high value proteins from particle containing potato fruit juice via direct capture membrane adsorption chromatography. *J Biotechnol* 168: 693-700
 21. Galier S, Balmann HR-d (2011) The electrophoretic membrane contactor: A mass- transfer-based methodology applied to the separation of whey proteins. *Separ Purif Technol* 77: 237-244
 22. Zeman JL, Zydny LA (1996) Microfiltration and ultrafiltration: Principles and applications, Taylor & Francis
 23. Saxena A, Tripathi BP, Kumar M, Shahi VK (2009) Membrane-based techniques for the separation and purification of proteins: An overview. *Adv Colloid Interface Sci* 145: 1-22
 24. Lin JC-T, Lee D-J, Huang C (2010) Membrane fouling mitigation: Membrane cleaning. *Separ Sci Technol* 45: 858-872
 25. She Q, Tang CY, Wang Y-N, Zhang Z (2009) The

- role of hydrodynamic conditions and solution chemistry on protein fouling during ultrafiltration. *Desalination* 249: 1079-1087
26. Hermans P, Bredée H (1936) Principles of the mathematical treatment of constant-pressure filtration. *J Soc Chem Ind* 55: 1-4
 27. Bolton G, LaCasse D, Kuriyel R (2006) Combined models of membrane fouling: Development and application to microfiltration and ultrafiltration of biological fluids. *J Membrane Sci* 277: 75-84
 28. Bowen WR, Jenner F (1995) Theoretical descriptions of membrane filtration of colloids and fine particles: An assessment and review. *Adv Colloid Interface Sci* 56: 141-200
 29. Ng CY, Mohammad AW, Ng LY, Jahim JM (2014) Membrane fouling mechanisms during ultrafiltration of skimmed coconut milk. *J Food Eng* 142: 190-200
 30. Hermia J (1982) Constant pressure blocking filtration law application to powder law non-Newtonian fluid. *Trans Inst Chem Eng* 60: 183-187
 31. Hwang K-J, Liao C-Y, Tung K-L (2007) Analysis of particle fouling during microfiltration by use of blocking models. *J Membrane Sci* 287: 287-293
 32. Rai C, Rai P, Majumdar GC, De S, DasGupta S (2010) Mechanism of permeate flux decline during microfiltration of watermelon (*citrullus lanatus*) juice. *Food Bioprocess Technol* 3: 545-553
 33. Jafarzadeh Y, Yegani R (2015) Analysis of fouling mechanisms in TiO_2 embedded high density polyethylene membranes for collagen separation. *Chem Eng Res Des* 93: 684-695
 34. Jafarzadeh Y, Yegani R, Sedaghat M (2015) Preparation, characterization and fouling analysis of ZnO /polyethylene hybrid membranes for collagen separation. *Chem Eng Res Des* 94: 417-427
 35. Golbandi R, Abdi MA, Babaloo AA, Khoshfetrat AB, Mohammadalou T (2013) Fouling study of TiO_2 -boehmite MF membrane in defatting of whey solution: Feed concentration and pH effects. *J Membrane Sci* 448: 135-142
 36. Meng H, Cheng Q, Li C (2014) Polyacrylonitrile-based zwitterionic ultrafiltration membrane with improved anti-protein-fouling capacity. *Appl Surf Sci* 303: 399-405
 37. Kumar M, Ulbricht M (2014) Low fouling negatively charged hybrid ultrafiltration membranes for protein separation from sulfonated poly(arylene ether sulfone) block copolymer and functionalized multiwalled carbon nanotubes. *Separ Purif Technol* 127: 181-191
 38. Bowen WR, Calvo JI, Hernández A (1995) Steps of membrane blocking in flux decline during protein microfiltration. *J Membrane Sci* 101: 153-165
 39. Ho C-C, Zydny AL (2000) A combined pore blockage and cake filtration model for protein fouling during microfiltration. *J Colloid Interface Sci* 232: 389-399
 40. Shokri E, Yegani R, Heidari S, Shoeyb Z (2015) Effect of PE-g-MA compatibilizer on the structure and performance of HDPE/EVA blend membranes fabricated via TIPS method. *Chem Eng Res Des* 100: 237-247
 41. Ahsani M, Yegani R (2015) Study on the fouling behavior of silica nanocomposite modified polypropylene membrane in purification of collagen protein. *Chem Eng Res Des* 102: 261-273
 42. Nandi B, Das B, Uppaluri R (2012) Clarification of orange juice using ceramic membrane and evaluation of fouling mechanism. *J Food Proc Eng* 35: 403-423
 43. Wakeman RJ, Williams CJ (2002) Additional techniques to improve microfiltration. *Separ Purif Technol* 26: 3-18
 44. Shirazi S, Lin C-J, Chen D (2010) Inorganic fouling of pressure-driven membrane processes - A critical review. *Desalination* 250: 236-248
 45. Wright A, Thompson M (1975) Hydrodynamic structure of bovine serum albumin determined by transient electric birefringence. *Biophys J* 15: 137-141